2019

Wind Turbine Technical Report

Iowa State University

Team Members

Aerodynamics Team	Electrical Team	Mechanical Team
Cody Hornyak	Julia Zhang	Thomas Polzin
Kathyrn Paszkiewicz	Joe Paffrath	Sam Fletcher
Brian Caskey	Abdel Rahman Mannan	Luis Arce
Joseph Nyakamwe	Dylan Miley	Collin Wendt
	Hieu Nguyen	Jorge Gomez

Team Lead: David Jordan

Strategic Advisers: Dr. Sri Sritharan, Nicholas David

Table of Contents

1. EXECUTIVE SUMMARY 2

2. TECHNICAL DESIGN 2

2.1 Design Objective 2
2.2 Mechanical Design 3
2.2.1 Tower 3
2.2.2 Yaw 3
2.2.3 Tail 4
2.2.4 Nacelle 5
2.2.5 Blades 5
2.2.6 Pitch System 7
2.3 Electrical Design 8
2.3.1 Generator 8
2.3.2 Power Converter 10
2.3.3 Load Model 11
2.3.4 Control System 12
2.3.5 PID Tuning 15

3. TESTING RESULTS 15

3.1 Electronic Bench Testing 15
3.2 Wind Tunnel Testing 16

4. CONCLUSION 17

5. APPENDIX 18

5.1 Power Control Derivation Equations 18
5.2 Speed Control Derivation Equations 18
5.3 Exploded View of Turbine Parts 18

5.4 POWER CONVERTER DETAILED SCHEMATIC 19

6. REFERENCES 20

1. Executive Summary

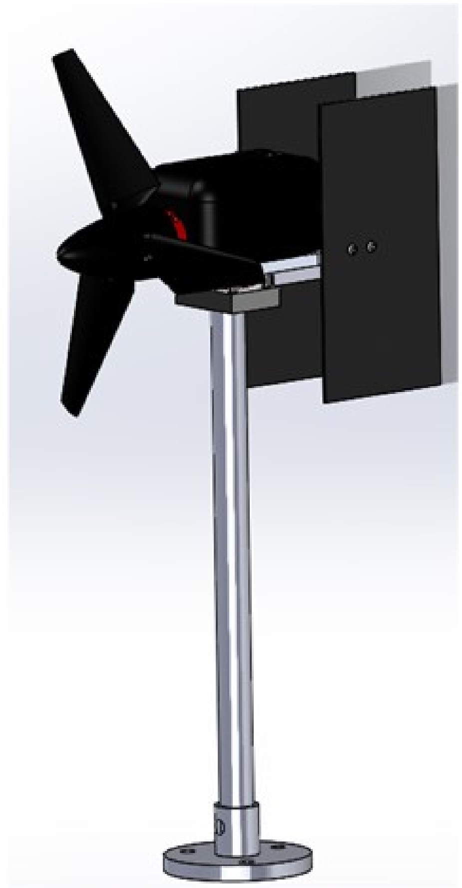

Figure 1: SolidWorks model of the completed turbine

The Wind Energy Team at Iowa State University (ISU) has designed and built a turbine for the DOE Collegiate Wind Competition (CWC). Over the course of two semesters, the team has worked to improve upon the foundation of the 2018 project and capitalized on the lessons learned from that competition. There are similar aspects to the turbines of both years, but most major systems in the 2019 turbine have been reengineered.

The turbine is a three bladed, horizontal axis wind turbine that is designed to spin up to 2500 rpm and to produce 37.5 W at 11 m/s wind speed at a geographic elevation of 942 feet in Ames, IA. The prototype, as seen in Figure 1, has a passive yaw system that uses a tail to direct itself into the wind. For power transmission, the blades rotate the low speed shaft which is connected by a timing belt system with a 3:1 gear ratio to a high-speed shaft attached to the Multistar Elite 3508 permanent magnet synchronous generator. The turbine has an active pitch system with a single linear actuator that allows the blades to rotate in and out of the wind. The turbine also has an rpm sensor that reads the angular speed of the hub. Knowing the speed allows the turbine to use the pitch system to regulate power output and rotational speed. During extreme wind speeds, the blades can be pitched to a stall angle, causing the hub to stop rotating. The power produced from the turbine charges a 12V 10AH lithium iron phosphate battery. After the functional designs were finalized, the team made a nose cone and nacelle cover to help contain the turbine components and enhance its aerodynamic behavior.

Multiple designs for the turbine have been modeled, built, and tested, thereby a system was optimized. During the design process, the team has used programs such as SolidWorks, Q-Blade, MATLAB and Simulink for modeling, ANSYS and XFLR-5 for analysis, Excel for logging and plotting data, and Altium ProtelDXP and Arduino for coding. All designs have been verified by the software programs listed and physical testing in wind tunnels. Physical testing was conducted in an open circuit, single speed (8 m/s) wind tunnel built by the team and in ISU's closed-circuit Aerodynamic/Atmospheric Boundary Layer tunnel (AABL). Testing has shown that the newly designed turbine will successfully go through tests planned as part of the 2019 competition.

2. Technical Design

2.1 Design Objective

In the 2018 competition, there were issues with mechanical components breaking and electrical components not functioning correctly. This year, the team made reliability and efficiency the major focuses for the design. Mechanically, the team strove to have a minimum factor of safety of two for parts and connections. In addition, the team wanted a blade that can produce as much torque as possible while limiting the amount of drag in order to maximize the power production. For electrical components, the team worked on improving the efficiency and regulation of power conversion. All these key aspects were emphasized holistically, so that the turbine can reliably produce as much power as possible.

2.2 Mechanical Design

2.2.1 Tower

The alloy steel tower was designed with simplicity and safety in mind. The horizontal base plate is 16 millimeters in thickness, 150 mm in diameter, and is secured to the tower using a 12.7 mm thick collar. A 38.1 mm diameter tube with a thickness of 12.7 mm was chosen for the tower. The wires from the turbine run through the tube and out a hole in the bottom of the tower. With the base plate, a tower height of 0.61 meters was chosen to keep the nacelle within the designated height range. A max wind speed of 20 m/s and a solid circular blade-swept area would keep displacement at the top of the tower below 1.7 mm. The maximum stress in the tower is expected around the hole in the tower collar. As shown in Figure 2, this tensile stress will not exceed 42 MPa, which produces a safety factor of nearly 6 when the yield strength is 250 MPa [4].

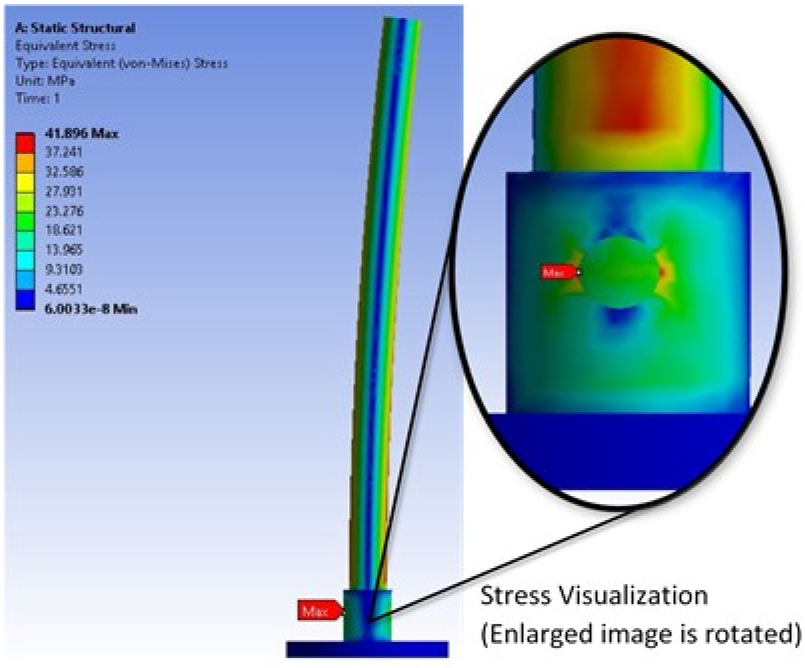

Figure 2: The tower stress analysis as modeled in ANSYS

2.2.2 Yaw

The turbine utilizes a passive yaw system, so the wind may keep the structure in line. The components of the system are shown in Figure 3 and function as follows. First, the nacelle base plate acts as the foundation to most of the turbine components, as the turbine's parts are mounted to it. The plate needs to rotate freely so that the blades can be aligned in the wind. The nacelle base plate sits on top of one of two needle roller thrust bearings. This bearing reduces friction between the nacelle base plate and the shaft collar. The shaft collar is secured to the tower with a set screw and is the main connection point between the turbine and the tower. Underneath the collar is the second needle roller thrust bearing, which sits on top of the yaw bearing housing. A needle roller bearing is press fit in the center hole of the yaw

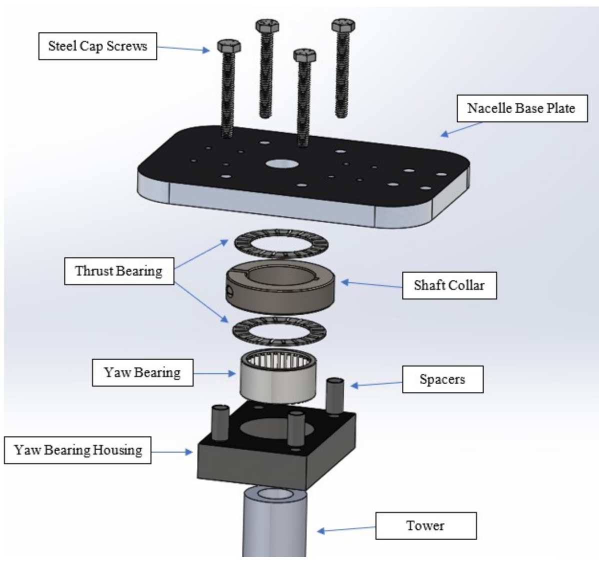

Figure 3: Exploded view of the yaw assembly

bearing housing. This bearing allows the turbine to rotate about the tower and yaw with the wind. The thrust bearings, yaw housing, and shaft collar all fit around the tower and are held together by four Grade 8 1/4-20 steel cap screws that run down through the nacelle base plate and yaw bearing housing, as shown in Figure 4. After the initial design, it was found that tightening the nuts caused too much friction in the thrust bearings, which significantly affected the response of the yaw, and without tightening, the nuts would unscrew and fall off. To solve this issue, the team added spacers made of 9.5 mm aluminum tubing that the screws slide through. These spacers were made with a clearance of twenty thousandths of an inch, so that the nuts and screws compressed the spacers and not the bearings. The spacers alleviated the friction on the thrust bearings and allow the turbine to spin freely about the tower. Overall, the yaw system allows the turbine to rotate about the tower and secures the nacelle.

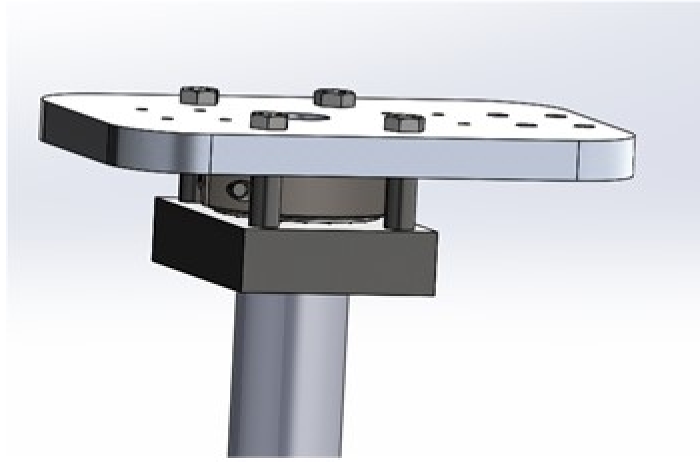
Figure 4: The assembled yaw system put

2.2.3 Tail

The yaw system allows the turbine to spin, but the tail must align the turbine in the wind. For the design, the goal was to optimize the tail allowing the turbine to yaw into the direction of the wind and keep it there. According to [8], a passive yaw turbine should have a tail that has a surface area of 20% of the swept area of the blades. Using this information as a guide, an initial tail design was a triangular shaped plate with a 30-degree angle of inclination and had a surface area of 274.8 cm^2. However, during testing, the aerodynamic imbalances of the turbine caused it to yaw out of the wind. This made the team reevaluate the tail design, which led to increasing the surface area of the tail significantly. To accommodate the desired increase in surface area, the new design features two parallel, rectangular tails, as seen in Figure 5. Each tail has a surface area of 961.3 cm^2 and is made of 3.175 mm thick aluminum. The tail pieces are connected to two pieces of aluminum T-slotted bracing using 1/4-20 socket cap screws. The bracing pieces attach to 90-degree brackets that are connected to the bottom of the nacelle plate with 1/4-20 steel screws. The dual tail design also allows room for the linear actuator to have a sturdy mount.

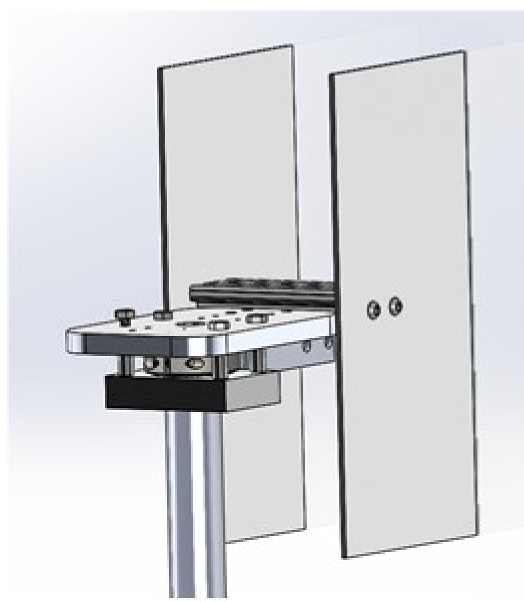
Figure 5: The design of the tail

2.2.4 Nacelle

For the nacelle design, the team focused on reliability and adjustability. The low speed shaft, made of aluminum, is kept in line by two pillow blocks that are fastened to the nacelle plate. For power transmission, the turbine uses an MXL series timing belt and pulleys. The low speed shaft spins a pulley with 60 teeth that transfers the power from the blades to the generator via another pulley with 20 teeth. The two pulleys have a 3:1 gear ratio and use a 6.35 mm wide timing belt. The generator is mounted on a bracket that is secured to a piece of 25.4 mm T-Slotted aluminum bracing, which is bolted to the nacelle plate. The bracing allows the generator to be adjusted easily from side to side so that the timing belt can be aligned and tensioned properly. To pitch the blades, the turbine uses a linear actuator that is mounted to the same bracing where the tail is mounted. The slotted aluminum allows the linear actuator to be aligned easily. There is a linear bearing held in place by two mounts, which are secured to the base plate, that allow the pitch rod to slide back and forth through the low speed shaft. Also, there is a radial bearing with a large tolerance, which allows it to act like a linear bearing, that is mounted in the front of the low speed shaft in the hub. These bearings allow the pitch rod to be supported in three places along its length (at both bearings and at the connection to the actuator) and to slide through the low speed shaft with minimal friction.

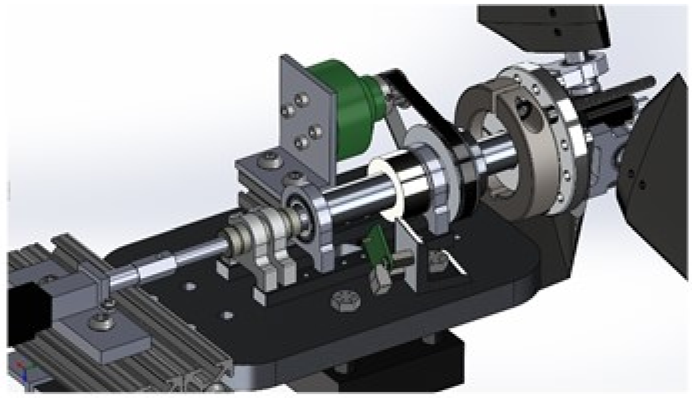

Figure 6: The layout of the nacelle and its components

2.2.5 Blades

The process of the blade design began with research to find the most effective design that will also minimize cost and weight. Online research found many academic papers that explained airfoils used in industrial turbines. It was difficult to find information on design of micro-scale blades, specifically as small as the dimensions allowed in CWC. The literature led the team to start with low-Reynolds number airfoils and gave general blade shapes based on target tip speed ratios (see Figure 7).

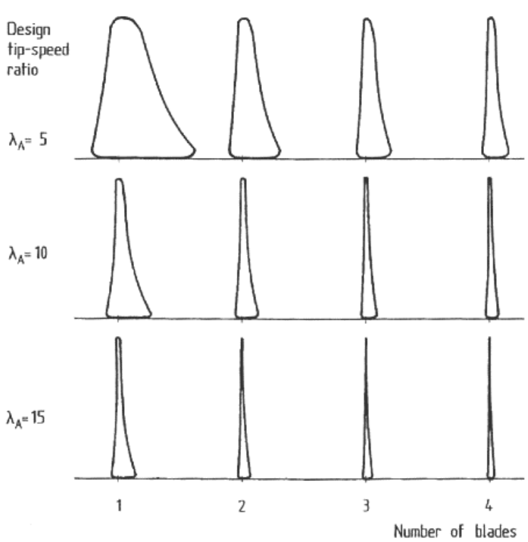

Figure 7: Tip speed ratio for different air foils

After the initial design, the team consulted faculty on campus who have worked with the design and optimization of wind turbine models. In discussion with Dr. Hui Hu and Dr. Partha Sarkar of the Aerospace Engineering Department, the team realized the importance of incorporating an angle of twist, which was not included in the initial designs of the blades. The team then moved forward with researching what twist angles would be optimal for the different design ideas.

It was determined that the generator needed to rotate at 6000 rpm for the most efficient power production. The team found the gear ratio from the high-speed to the low-speed shaft is 3:1, making the target rpm for the blades 2000. Knowing the competition restricts blade diameter to 45 cm, the tip speed ratio, λ, was designed as follows:

$$v_{\text{tip}} = \omega r = 2000\frac{\text{rev}}{\text{min}} * 2\pi\frac{\text{rad}}{\text{s}} * 60\frac{\text{min}}{\text{s}} * 0.225\text{m}=47.13 \text{ m/s}$$

where v_{tip} is the velocity of the blades at the tip, ω is the angular velocity of the blade rotation, and r is the radius of the blade sweep. By dividing the blade tip speed by the blade wind speed of 11 m/s, the tip speed ratio can be found as:

$$\lambda_{11\text{m/s}}=4.27$$

After research on the design of turbine blades and the significance of each design parameter, airfoils were chosen, allowing the team to draft different blades and gauge their performance using computer simulation.

The primary method of performance analysis used was Q-Blade, an open-source software. Q-Blade uses XFLR5 to analyze airfoil performance at 360 degrees angle of attack and then allows the user to draft blades from those airfoils in a 3D editor. After drafting a blade, Q-Blade can generate C_p vs. λ graphs for analysis, where C_p is the coefficient of power and λ is the tip speed ratio. After iterating in Q-Blade with respect to a variety of angles of twist and chord lengths, blade designs could be exported to SolidWorks. An addition in the SolidWorks model is a mechanism at the root for connection to the blade-stem (blade to hub). As seen in figure 9, this is a through-hole design to decrease the stresses and chance for tear-off stress failure. All blades were 3D-printed at the College of Design on a Lulzbot TAZ 5 and 6 printers with a composite plastic. The blades were then fit with a blade stem and attached to the hub for testing.

The second method of performance analysis was experimental testing. Several sets of blades were printed with different designs, including a NACA 4421 airfoil straight loft, an SD 7034 straight loft, and a NACA 4421 airfoil with a 20° angle of twist. Designs were tested in the AABL Wind and Gust Tunnel in the Aerospace Department of Iowa State University, where the tunnel allowed for testing to be done in a range of wind speeds that align with the competition requirements. From these tests, the team was able to determine the cut in wind speed of the blade at different angles of attack and the power output at different conditions.

After the analysis and testing, a final blade was selected. The current blade design for the turbine is drafted from a NACA 4421 airfoil curve-lofted to an FX 63-137 airfoil. The FX family of airfoils are slimmer, therefore, more accommodating to tip speed ratio and rpm count that the team desired. The angle of twist on the final blade design is 15°. This was selected based off the optimal angle of attack of the un-twisted blade. The team used the on-campus 3D printer because the plastic held up well at speeds up to 20 m/s in the AABL wind tunnel. The final blade is shown in Figure 8 and 9, including the C_p vs. λ graph in Figure 13, where it can be seen the deliberate placement of the C_p peak at a tip speed ratio of 4.

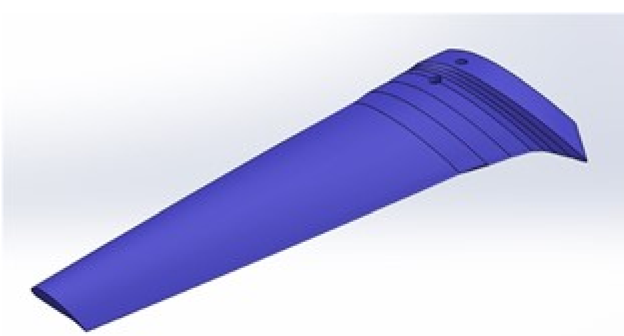

Figure 8: Isometric view of the blade

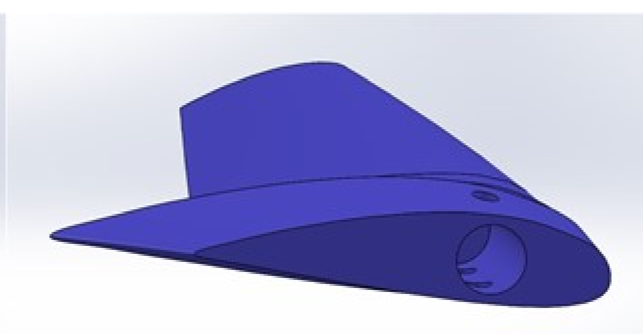

Figure 9: View of the blade that shows angle of

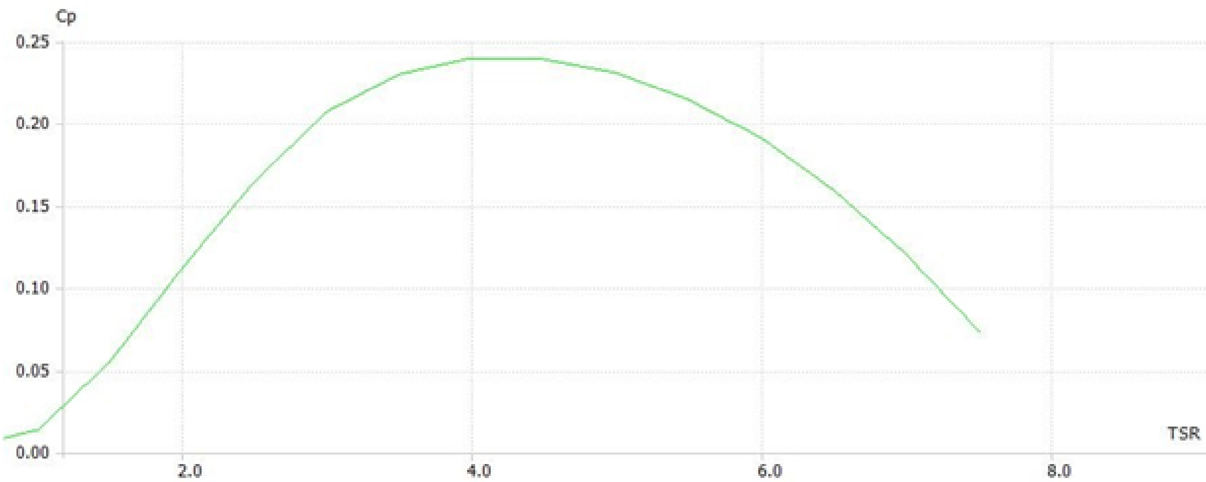

Figure 13: Tip Speed Ratio (TSR) vs. Cp plot

A nose cone was designed to cover the components in the nose. Though a nose cone does not offer much overall drag reduction at such low windspeeds, it does keep the incoming flow off the pitch block and offers relief to the linear actuator when pitching the blades forward.

Wind tunnel testing found an unwanted yaw as windspeed increased. This yaw was found to be caused by a drag imbalance due to the side-configuration of the generator. To fix this, a nacelle cover was designed to fit over the entirety of the nacelle to balance the drag. This nacelle cover was drafted in SolidWorks and then 3D printed.

2.2.6 Pitch System

As mentioned in Section 2.2.4, the pitch system uses a linear actuator mounted in the rear of the nacelle to push the pitch rod forward and backward, which rotates the blades. A pitch block, which is made of 3D printed ABS plastic (the black triangular piece in Figure 14) holds a small section of 48 diametral pitch (DP), 20-degree pressure angle (PA) brass (gear) rack. The rack engages a 48 DP, 20-degree PA 303 stainless steel pinion gear with hub and set screw that is fixed to the end of the blade stems. The blade stems connect the gear to the blade and are fixed to the blades with two 6-32 steel screws with nuts tightening them. The blade stems were machined from 9.5 mm aluminum rod stock, and the team turned down a 9.5 mm length to 4.7 mm diameter for the gear to fit onto.

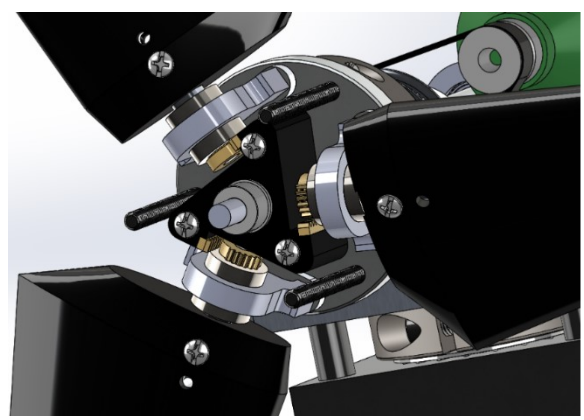

Figure 11: The pitch assembly in the hub

The teeth of the gears and racks are kept engaged with three springs stretching between screws on the pitch block and screws on the hub. The pitch system was designed to have 180 degrees rotation; however, the turbine only needs about 100 degrees of rotation. The extra rotation was added in case of any mechanical conflict with controls in the future. The blades are held in place by three pillow block bearings that the blade stems fit through. Two steel shaft collars are clamped on to the stem to hold the blade in place so that the gears can remain engaged.

To find the centrifugal force that acts on the blades and to see if the blades would theoretically last in 2500 rpm conditions, Equation 1 was used

$$F = m * \omega^2 * r \tag{1}$$

where *F* is the centrifugal force, *w* is the rotation speed of the hub, and *r* is how far from the center the force acts. The shaft collar used can experience up to 2668.9 N of axial (centrifugal) force before slipping, and from equation 1 when *m* = .111 kg, *w* = 267.1 rad/s, and *r* = 0.0889 m, the total force the collar will experience at the maximum speed is 676.7 N. This gives a safety factor of 3.9.

Another potential failure mode is the blade to blade stem connection. There are two screws that go through the blade and blade stem to hold them together. Based on the axial force from the equation above and the area that the screws touch on the blade, the stress experienced on the plastic is 9.86 MPa. The yield strength of the plastic is 28.5 MPA, so the safety factor is 2.89 [2].

2.3 Electrical Design

The electrical system displayed in Figure 12 consists of a generator, buck-boost power electronic converter, load, actuators and sensors, and relays. Two different controllers are utilized one for speed control and another for power.

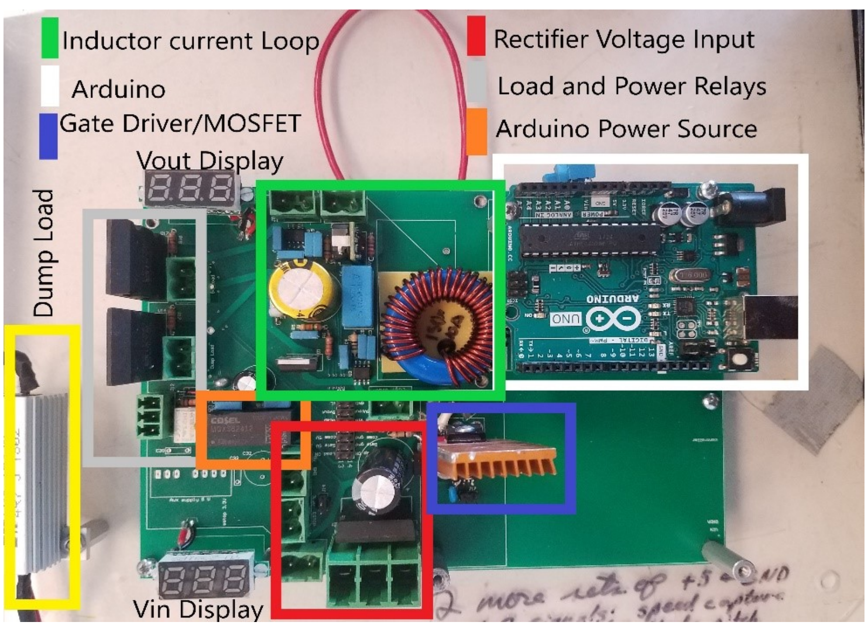

Figure 12: Power converter section diagram

2.3.1 Generator

Using experience from the 2018 Collegiate Wind Competition, the Turnigy Multistar Elite 3508 generator was chosen as it was found to have sufficient power, speed, and voltage range for the turbine (see Table 1). This permanent magnet synchronous generator was tested under speed and loading conditions using a second machine as a prime mover with open-loop servo drive.

Table 1: Generator Nameplate Properties

K_v (rpm/v)	268
Power (W)	330
Unit Weight (g)	83
Max Current (A)	12
Max Voltage (V)	35

The first test performed was to confirm the number of magnetic poles in the PMSG. Using a prime mover motor, tachometer, and oscilloscope with differential voltage probes, the line-to line terminal voltage was measured across the generator speed range. The data from Table 2 was plotted and the slope calculated with a linear regression using MATLAB. The machine was determined to have 14 poles.

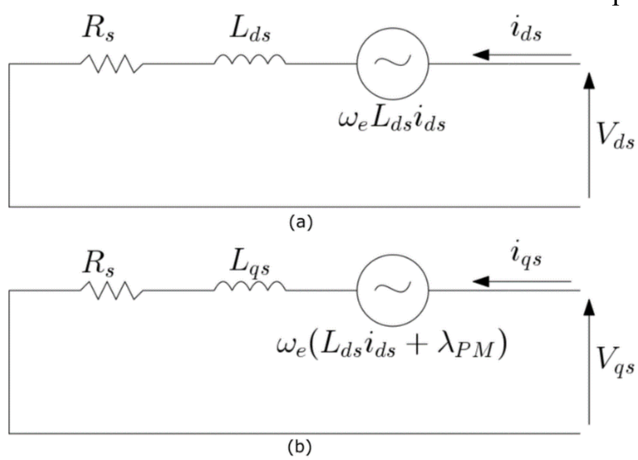

Figure 13: Generator electrical model

Table 2: Generator testing data for parameter identification

Mechanical Rotational Speed, ω_{rm} (rpm)	Line-to-Line Terminal Voltage (V)	Period, T (s)	Calculated Frequency, f 1/T	Calculated Electrical Speed (rad/sec)
918	2.75	0.0092	108.7	682.9
1830	5.30	0.0046	215.5	1354.1
2773	8.20	0.0027	365.0	2293.1
3625	10.7	0.0024	423.7	2662.4
4505	13.2	0.0019	526.3	3306.9
5354	15.7	0.0016	625.0	3927.0

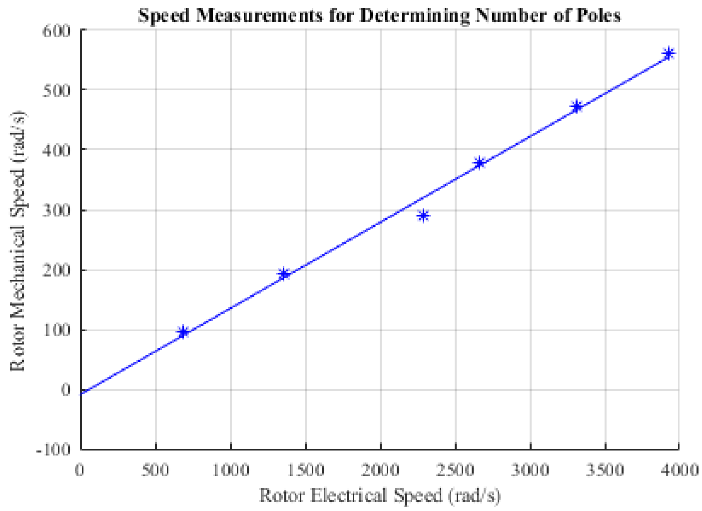

Figure 14: Plot of rotor electrical vs. mechanical speed

The data of Table 2 was also used to find the magnetic flux constant. The open-circuit terminal voltage varies with rotor speed and has value that is in proportion to the flux. The measured slope indicates a flux constant of .0023 V/rad/s.

2.3.2 Power Converter

The goal of the power conversion system is to read the existing input and output voltage and command current in order to achieve a desired power. An efficient way of accomplishing this task involves the use of a buck-boost converter and was built by the team. Considering the design form 2018, many improvements were made, which included moving to a printed circuit board and minimizing power taken by switching devices for added efficiency. Overall the converter is 80% efficient when bench testing and has a two to three watt power loss in order to run the controller.

Generator input-stage: rectifier and power supply

The system starts by taking a three phase AC input and converts it to a DC voltage source through a three-phase bridge rectifier [*FUS45-0045B*] attached to a capacitor to help smooth out the voltage. Attached as well to the input-stage is the Arduino power supply that takes an input of 6-60V in order to power the Arduino, linear actuator, and power electronic components. The maximum rectified DC voltage found through testing does not exceed 30V when load is applied on the generator and under 35V when unloaded. A voltage divider is used to monitor the input voltage and also in control of the duty cycle. An overvoltage triggers a safety-state and the gate driver is shut off by commanding a 0% duty cycle and the user is flagged of the issue via a serial monitor.

Microcontroller, Actuator and rpm Sensor

The system relies on an Arduino Uno micro-controller to operate the pulse width modulation (PWM) functions that drive the buck-boost converter and also the pitch system's linear actuator. It reads all the sensors every time the code loops, trigger different control states, switch relays, and calculate the power to control. After bench testing with the actuator 150 nF capacitors were added to filter the analog inputs that the microcontroller received.

A 12V linear actuator[*L12-I*] ordered was chosen due to its small size and fast speed for the force needed to actuate at up to 20 m/s wind speed. Additionally, it uses the same power supply voltage as the Arduino which simplifies design and reduces cost. Using the equation Force = $Q*A*C_d$ where A is the rotor area, Q is the dynamic pressure and a drag coefficient of 0.14 as an estimate to represent the blades at a large angle of attack, a max load of approximately 7.8 N was found and the fastest actuator was chosen appropriately for this scenario. The other electrical component on the turbine is a Sunfounder hall effect sensor used to sense the change in magnetic field. With every control-loop iteration the Arduino counts as to how many times the magnetic field has passed in front and then converts that value to an rpm. After testing, a low-pass filter in the code was added to achieve a smooth value.

Buck Boost Converter

The main buck boost follows the typical buck-boost schematic with a inductor, diode, capacitor, and MOSFET with gate driver as shown in Figure 15. The power is then regulated in the output of the converter through controlled inductor current. All of these components were chosen with the goal of making a 10A step change in the inductor current. The gate driver is controlled by a PWM signal sent to it by the Arduino and operates on a 32 kHz switching frequency. As the gate driver is turned on and off according to the duty cycle, the current flows through the inductor and charges the output capacitor. The output is then used with the team's load or to power another 5 V regulated output as used in the durability task of the competition. The design utilizes a Schottky diode to minimize the voltage drop at the output stage [*STPS30100ST*]. Over-voltage and current protection were also added to the Arduino code running the converter and commands the duty cycle to zero if more than 15V were measured at the output and/or more then 8A was measured through the inductor. It was then through bench testing with a thermal camera that the MOSFET and the Schottky diode needed a heatsink. This was shown by the static drain resistance term R_{ds} of the old MOSFET was rising to 0.5 ohms and drawing 2 watts of power at 150^o C. A change in the MOSFET was made and the current MOSFET has a max R_{ds} of .0382 ohms [*FDPF3860T*].

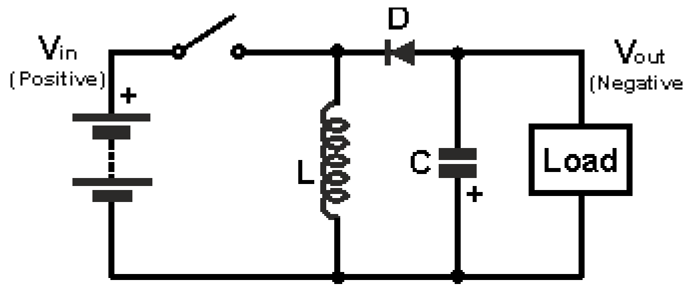

Figure 15: Buck boost converter topology

Relays and Dump Load

Load-control relays are the final key component of the electrical power conversion hardware. In order to take advantage of the power available at both the input and output sides of the converter, a double pole double throw power relay [*3-1462039-0*] was placed before the Arduino power supply; the normally closed terminals are attached to the rectifier side input. The Arduino can switch the relay to power itself from the load or supercapacitor in case no power is available from the wind. This approach will be useful during the safety tasks when the turbine needs to operate the pitch actuator. Two open-collector solid-state relays [*CPC1709J]* controlled through the Arduino are attached before the load and the dump load which are normally off to avoid power draw until the turbine gets up to speed. The dump load was added to the system to avoid any possible risk of being at a very high wind speed and having the supercapacitor fully charged. The 4.7ohm dump load resistor is capable of draining 47.9 watts which is out of the maximum load prescribed in the competition rules.

2.3.3 Load Model

The load for the turbine is both practical and innovative. A 12V 10AH lithium iron phosphate battery was chosen as they are a rechargeable battery for high power applications and a large amount of cycles. A Specifications of this battery are summarized in table 3. It can be seen that its characteristics are similar to those of the supercapacitor.

Table 3: Battery name plate parameters

	Lithium Iron Phosphate Battery	Competition Supercapacitor
Capacity/Capacitance	10 Ahr	58F
Max Charge Current	10 A	170 A
Nominal Current	5 A	
Charging Max Voltage	14 V	17 V
Discharging Max Voltage	9 V	17 V

The battery's nominal voltage of 12V lies in a sufficient range as to power the Arduino power supply. One thing the team has considered is a minimum discharge voltage as to not damage the battery. This means the minimal voltage is 2.8V * 4 cells so if the battery drops to 11.2 V the power relay will switch off the battery as to avoid damaging it. The relay will be normally off as to adhere to a zero-state of charge at the beginning of the test and switch on as soon as the Arduino is powered and has determined a load can be drawn. For the portion of the safety task where the load gets disconnected a current sensor on the output measures the load disconnection via current-change and the Arduino would trigger safety-state.

2.3.4 Control System

Two control loops have been designed for the turbine speed control used to change the pitch of the wind turbine's blades and a second is used in power control to command current to pass through the inductor which effectively regulates power. The control system is illustrated in Figure 16 as an engineering flow chart. From the cut-in wind speed of 5 m/s to 11 m/s the turbine operates with maximum power point tracking (MPPT) and at wind speeds above 11 m/s, the controller goes into a speed-controlled mode with constant power generation equal to the nominal value found at the 11 m/s. The control system utilizes an Arduino Uno that takes input data from the Hall effect sensor, a voltage sensor that reads the voltage on the input through the rectifier, a current sensor to read current through the inductor and a voltage sensor to read the output voltage. Through these sensors a few safety parameters were established. As long as none of the safety parameters are triggered the Arduino commands the control and is updated every time the code loops.

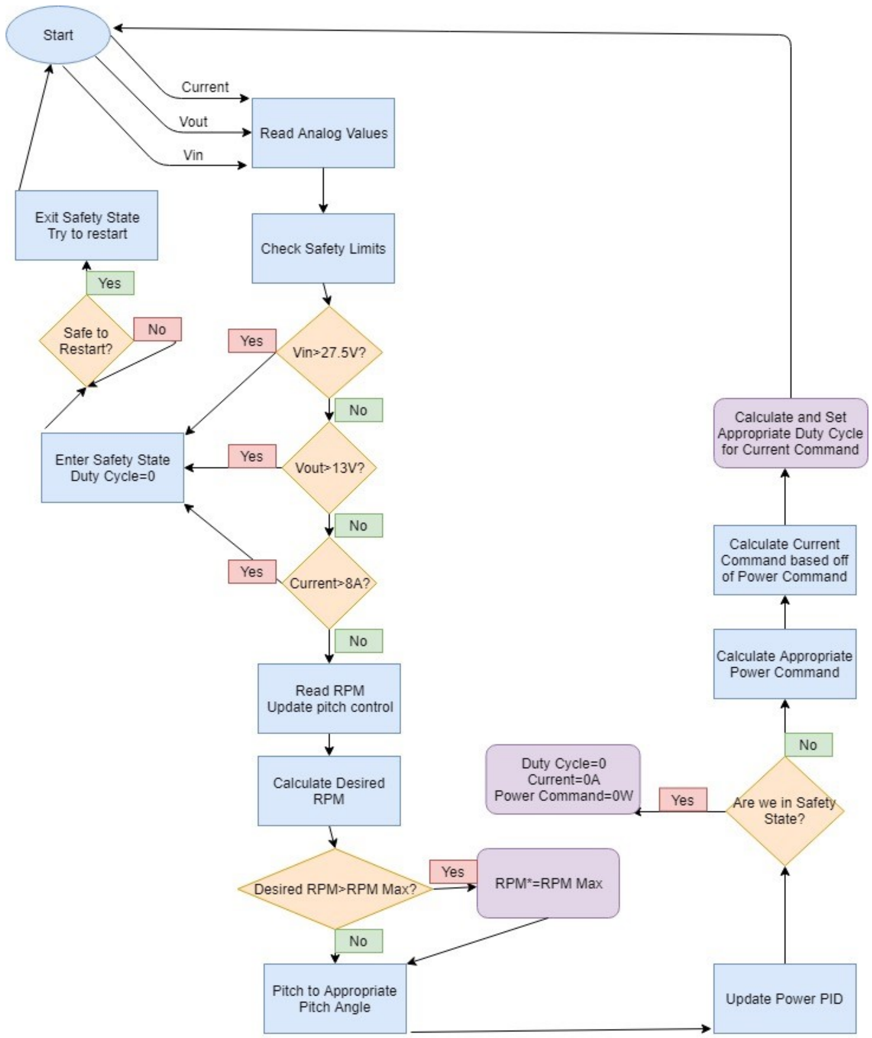

Figure 16: Control loop flow chart

Speed Control

The speed control is necessary for the control of rated speed above the 11 m/s wind speed and can overall increase the ability of the turbine to produce power effectively. The speed control method developed in Figure 17 for the turbine takes in a commanded speed and then changes the pitch angle with a linear actuator to regulate the speed. Equations to derive the speed controller are seen in the appendix and rely on a combination of Cp_{max} and λ_{opt} determined through testing. The derivations show the way to determine whether the system will need to accelerate or decelerate based on the current and is reflected in the code.

$$c_P < \frac{C_{P_{mat}}}{\lambda^2_{optimal}} \lambda^3 \rightarrow \dot{\omega} < 0 \text{ decelerate (too high tip speed ratio)} \tag{2}$$

$$c_P > \frac{C_{P_{mat}}}{\lambda^2_{optimal}} \lambda^3 \rightarrow \dot{\omega} > 0 \text{ accelerate (will stall)} \tag{3}$$

Power Control

The power control algorithm was first derived after analyzing an average state space model representation of the buck-boost system. By solving the buck-boost circuit for the change in current through the inductor diL/dt and change in voltage through the capacitor dVc/dt for each the on state when the switch is closed represented by the duty cycle (d) and the off state when the switch is open(1-d). The following equations were found. Next equation [1] was solved to find the duty cycle actual and then set equal to a commanded duty cycle value with a PI control incorporated, d* (2). When d = d*, then the control worked, and the il/il* transfer function was created to represent the system

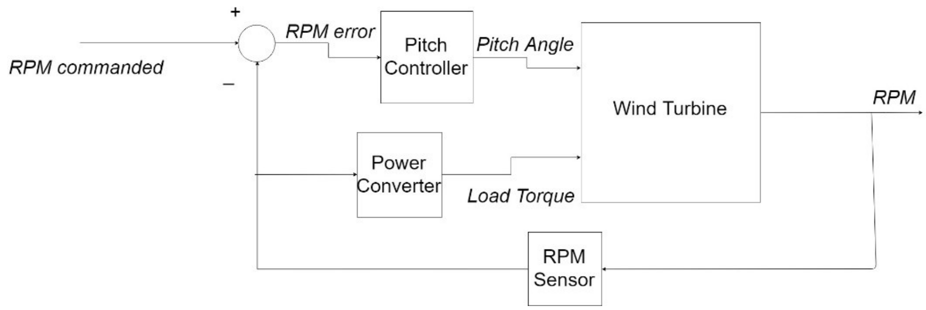

Figure 17: Speed control block diagram

$$d = \left(\frac{V_c}{V_s+V_c}\right) + \left(\frac{L}{V_s+V_C}\right) * \frac{di_L}{dt} \quad = \quad d^*(i_L^* - i_L)\left(K_p + \frac{K_i}{s}\right) + \left(\frac{V_c}{V_S+V_c}\right) \tag{4}$$

If control works, then $d = d^*$

$$TF\!: \frac{sK_p+K_i}{s^2\left(\frac{L}{V_S+V_C}\right)+K_p s+K_i} \tag{5}$$

Using the transfer function, the kp and ki terms were calculated through a process to solve for the poles and zeroes. With the use of the quadradic formula (Equation 6) was derived. When the term under the square root is set equal to zero the system has aa critically damped response and the natural frequency is the same for both poles. The rate of decay is determined by the magnitude of the pole so therefore directly associated with Kp. Then the Ki term is calculated in order to keep the critically damped response assuming that the Vs and Vc term are constant. All possible combinations of maximum and minimum V_s and V_c values were checked to assure stable response. However, while the simulation does give an overall picture for how the system responds final Kp and Ki values were decided after bench testing with the physical power converter, tuned to achieve current step-change of 0 to 4A.

$$s_{p_{1,2}} = -K_P \pm \sqrt{K_p^2 - 4\left(\frac{L}{V_s + V_c}\right)K_i} \tag{6}$$

Every time the code loops it calculates the current needed to flow through the inductor. First the code calculates the power to draw by taking in readings from the rpm sensor and calculates the power using formulas (Equation 7) where A is the constant rotor area, ρ is the air density, power coefficient C_p and tip speed ratio λ are related through an experimentally collected look up table, r is the rotor length , and omega is the rotor speed in rad/sec. This P value then gets divided by the measured V_{out} value when the switch is off and this duty cycle d is calculated through taking in measurements from V_{in} and V_{out} and rearranging the formula. Every time the loop runs the PI controller with a feedforward term takes in the i_l measured, calculates i_l* using the formula below and changes the duty cycle until the error is eliminated.

$$P = \frac{1}{2}\rho A C_p v_{wind}^3 \tag{7}$$

$$\lambda = \frac{r * \omega}{v_{wind}} \tag{8}$$

$$P = \frac{1}{2}\rho A C_p \left(\frac{r * \omega}{\lambda}\right)^3 \tag{9}$$

2.3.5 PID Tuning

The controller for commanding current through the inductor uses a PI controller to maintain a quick and stable jump in current with minimal or no overshoot. The controller was bench testing to determine appropriate values for the Kp and Ki values that the PI controller uses to determine how fast it allows current until it reaches the commanded value. The current system was used and current was manually commanded at different input voltages and in different magnitudes to experimentally find what the ideal values for these variables would be. The lower air density of the testing site in Colorado was also taken into account when determining appropriate values for Kp and Ki.

3. Testing Results

3.1 Electronic Bench Testing

The Wind Energy Systems Laboratory at Iowa State provided the team with some equipment and space to bench test some of the control's variables without a wind tunnel as illustrated in Figure 18. A programmable load, power supply, and oscilloscope were used in the lab to observe current jumps with different Kp and Ki values. The team would mimic generator conditions by experimenting with different variables and different jumps in power draw on the load to observe overshoot and speed of the current adjustment on the oscilloscope.

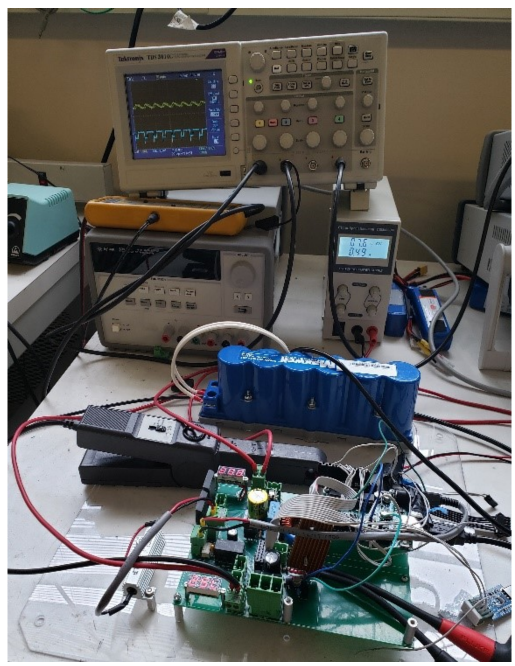

Figure 18: Setup of the bench testing for the

3.2 Wind Tunnel Testing

A custom cost-effective wind tunnel at the ISU's Applied Sciences Complex was built to test ideas quickly and easily. Using a shop fan and plywood, the constructed wind tunnel is capable of reaching wind speeds of 8m/s in a test.

Figure 19: Testing in the team's tunnel

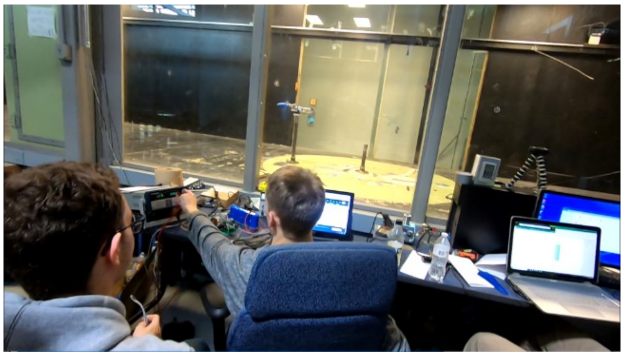

Figure 20: The team testing in the ABL tunnel

Additionally, the team was able to secure a week of testing in ISU's AABL tunnel. This wind tunnel allowed the team to emulate closely the conditions of the competition. With a full week of AABL tunnel access granted to the team, a myriad of electrical and mechanical problems was identified and fixed. Using a twisted version of the NACA blades, a power curve was found iterating through each blade pitch angle and competition wind speed. This data was then used to design the speed controller to control the pitch of the blades and regulate power production.

The ABL tunnel also contains a turntable inside the test section, and the team was able to test the turbine's yawing capability. First, as discussed previously an unwanted yawing occurred at higher windspeeds, and a nacelle cover was deemed necessary to balance the drag across the top of the turbine. It was also decided a new tail design was needed as the turbine was not yawing proficiently at lower windspeeds. Shown in Figures 24-26 are the values for C_p and λ for different wind speeds. It is through these plots that the trend of decreasing the angle of attack increases the overall power coefficient. This is only true to an extent because at speeds less then 11 m/s, the blades were stalling at low angles and therefore not producing any power. These values are incorporated into both the speed and power control through the use in the MPPT algorithm and the speed control logic. When the team tests at competition, these experimental values will need to be tuned in order to account for the approximate 20% loss of air density due to changes altitude through a trial and error process.

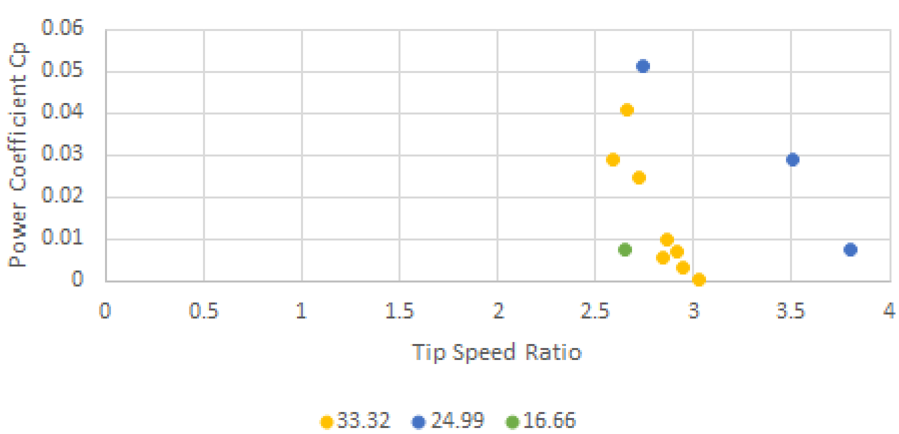

Figure 21: Cp vs. Lambda plot for 5 m/s for different angles of attack

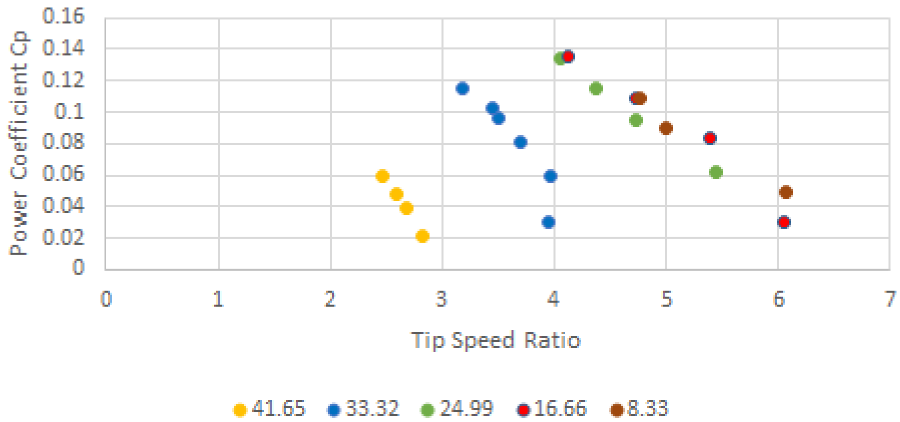

Figure 22: Cp vs. Lambda plot for 7 m/s for different angles of attack

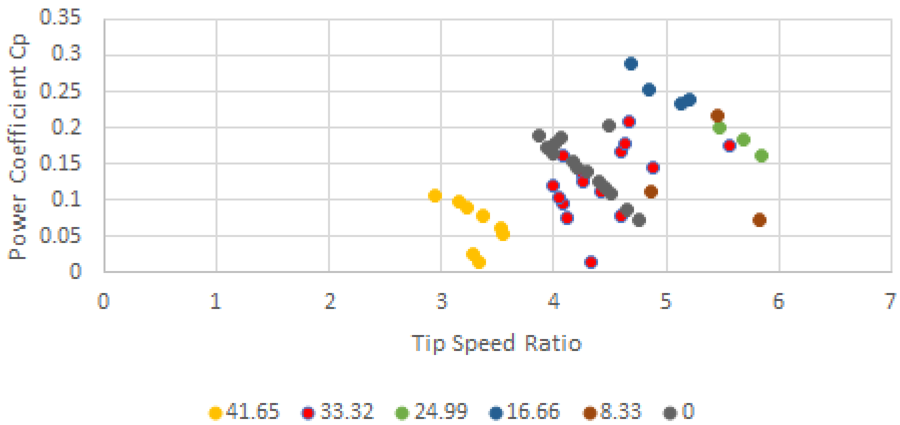

Figure 23: Cp vs. Lambda plot for 9 m/s for different angles of attack

4. Conclusion

This year the team has worked to engineer a turbine that is as efficient and reliable as possible. The product is a turbine that can produce 37.5 W at 11m/s. The turbine is able to regulate power and remain at 37.5 W at higher wind speeds because of the active pitch system. The hardware of the system utilizes a buck boost power converter for efficient power conversion and a microcontroller to control the linear actuator and read the sensors. Through the Arduino is software that uses a MPPT algorithm in order to determine the power to draw and a speed controller to regulate this power at high wind speeds while keeping rotor speed constant or slower. The control logic is dependent on the data collected through tunnel testing the team had accomplished at Iowa State's AABL tunnel and through the team's low-cost tunnel. Overall, the team is excited to compete in this competition, and is determined to utilize the learning and skills that the team has learned throughout the year.

5. Appendix

5.1 Power Control Derivation Equations

$d = \left(\frac{V_c}{V_s+V_c}\right) + \left(\frac{L}{V_s+V_C}\right) * \frac{di_L}{dt}$ - this is "actual

Here's the defined command: $d^*(i_L^* - i_L)\left(K_p + \frac{K_i}{s}\right) + \left(\frac{V_c}{V_S+V_c}\right)$

If control works, then $d = d^*$

$TF: \frac{sK_p+K_i}{s^2\left(\frac{L}{V_S+V_C}\right)+K_p s+K_i}$

$\frac{di_L}{dt} = \frac{(V_S\, d - V_C(1-d))}{L}$ [1]

$\frac{di_L}{dt} = \frac{\left(\frac{V_0}{R} d - \left(\frac{V_0}{R} - i_L\right)(1-d)\right)}{C}$ [2]

5.2 Speed Control Derivation Equations

$P = \tau\omega \Rightarrow \tau = \frac{P}{\omega}$ $\quad \lambda = \frac{wR}{V}$ $\quad V = \frac{\omega R}{\lambda}$ $\quad P = \frac{1}{2}\rho A C_P V^3$ $\quad \tau = \frac{1}{2}\frac{\rho A C_P (\frac{\omega R}{\lambda})^3}{\omega}$

$\tau_{aero} = \frac{1}{2}\rho\pi R^5 \frac{C_p}{\lambda^3}\omega^2$ at optimal λ $\qquad \tau_{command} = \frac{1}{2}\rho\pi R^5 \frac{C_p}{\lambda_{optimal}{}^3}\omega^2$

Now time derivative of ω $\alpha = \dot{\omega} = \frac{1}{J}(\tau_{aero} - \tau_L) = \frac{1}{2J}\rho\pi R^5\omega^2\left(\frac{Cp}{\lambda^3} - \frac{C_{P_{mat}}}{\lambda^3_{optimal}}\right)$

5.3 Exploded View of Turbine Parts

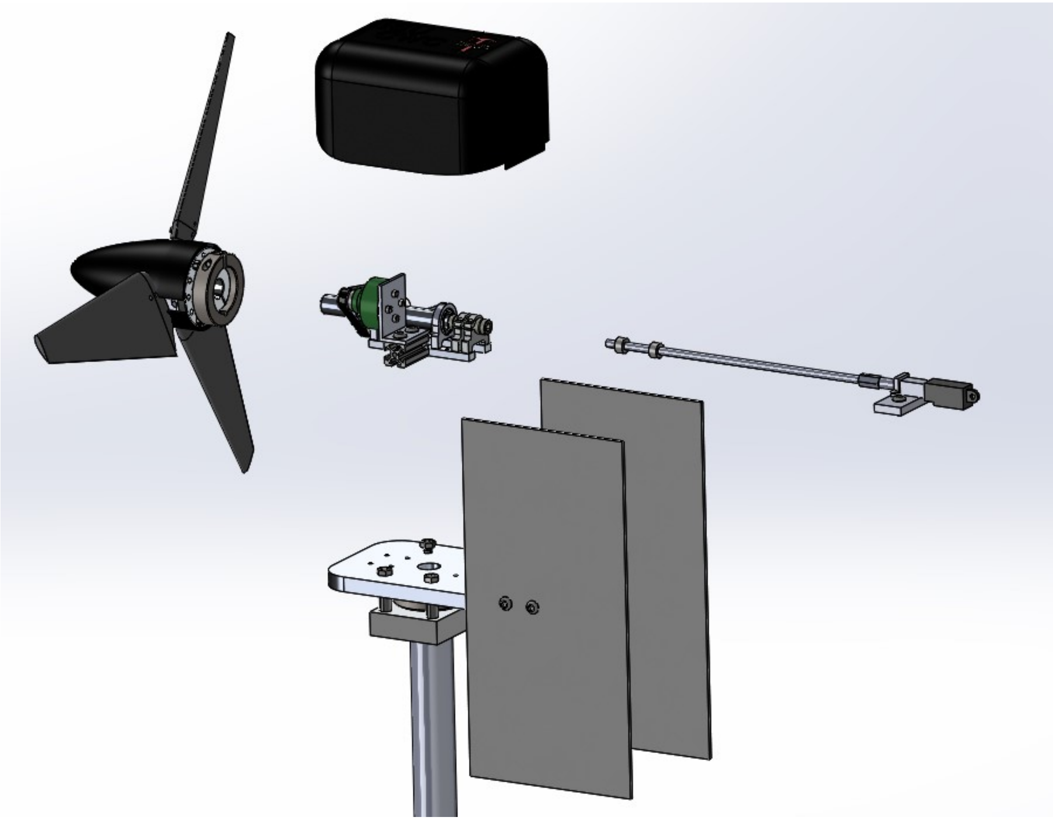

5.4 Power Converter Detailed Schematic

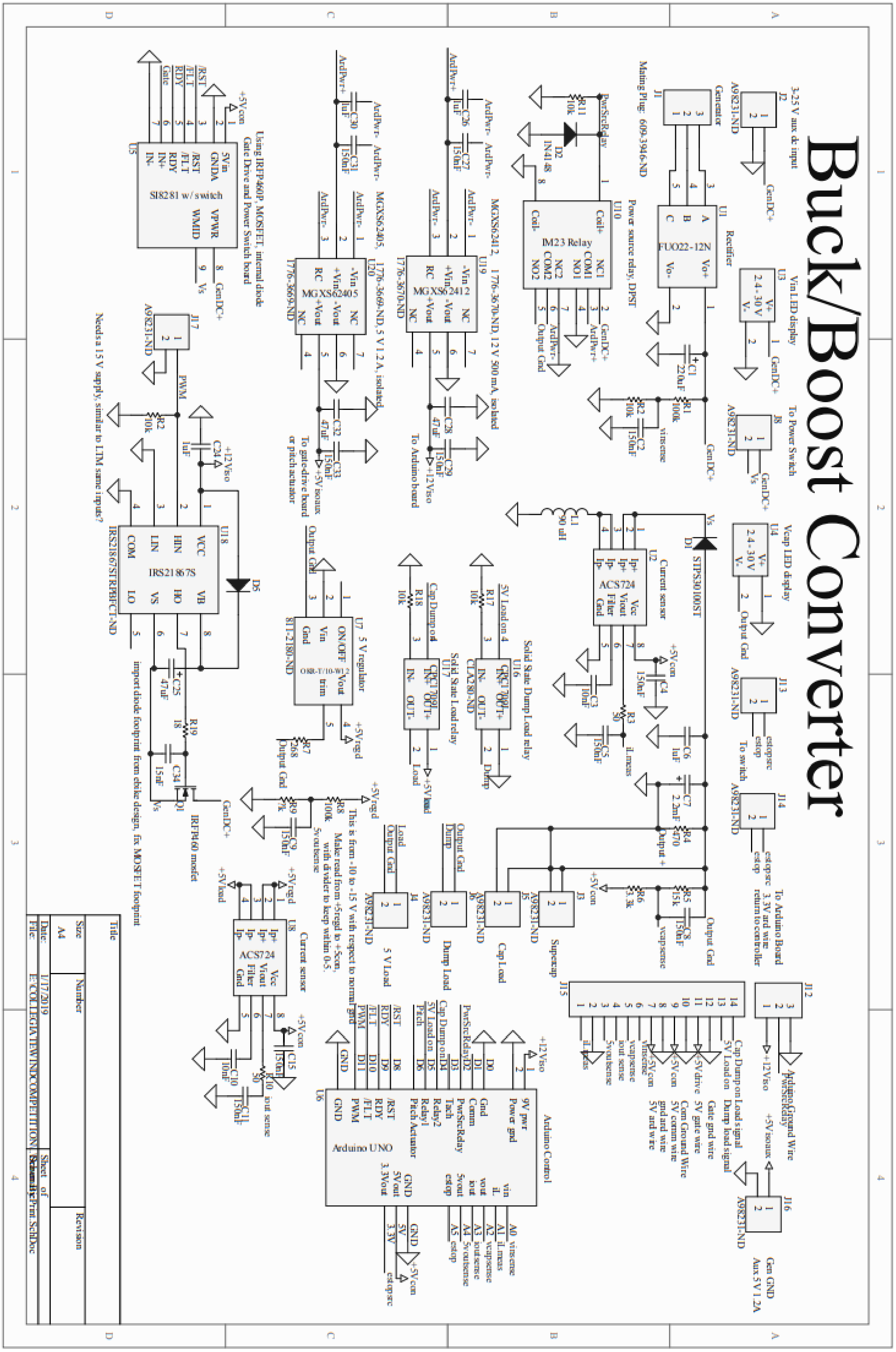

6. References

[1] Arduino Uno Rev3. (n.d.). Retrieved from https://store.arduino.cc/usa/arduino-uno-rev3
Coates, E. (2018, December 22). Module 3.3 Buck-Boost Converters. Retrieved from http://www.learnabout-electronics.org/PSU/psu33.php

[2] Cantrell, Jason, et al. Experimental Characterization of the Mechanical Properties of 3D-Printed ABS and Poly carbonate Parts. *Mechanical and Engineering Department University of Florida.* Retrieved from:http://web.mae.ufl.edu/rapidpro/pages/3D%20Printing%20Paper%20Final%20Manuscript.pdf

[3] Dakota Lithium 12v 10Ah Battery. (n.d.). Retrieved from https://dakotalithium.com/product/dakota-lithium-12v-10ah-battery/?v=7516fd43adaa

[4] Engineering Handbook Technical Information. *GI Huyett.* https://www.isibang.ac.in/~library/onlinerz/resources/Enghandbook.pdf

[5] Lihn, Christine M. (2015). Aerodynamic testing of micro-scale wind turbines. *The Pennsylvania State University College of Engineering,* 40-55.

[6] Multistar Elite 3508-268KV High Voltage Endurance Motor. (n.d.). Retrieved from https://hobbyking.com/en_us/multistar-elite-3508-268kv-high-voltage-endurance-motor.html

[7] NREL 5-MW Reference Turbine - CP, CQ, CT Coefficients. (n.d.). Retrieved from https://wind.nrel.gov/forum/wind/viewtopic.php?t=582

[8] Raikar, Nikhil C., Sandip A. Kale (2015). Effect of Tail Shapes on Yawing Performance of Micro Wind Turbine. *International Journal of Energy and Power Engineering.* Special Issue: Energy Systems and Developments. Vol. 4, No. 5-1, 2015, pp. 38-48.

[9] Selig, Michael S., et al. (1997). High-lift low reynolds number airfoil design. *Journal of Aircraft, 34,* 72-76.